ChemComm

COMMUNICATION

View Article Online
View Journal

Cite this: DOI: 10.1039/d5cc03528g

Received 24th June 2025,
Accepted 31st July 2025

DOI: 10.1039/d5cc03528g

rsc.li/chemcomm

Synergistic binary catholyte design for enhanced electrochemical performance in membraneless hybrid flow batteries

Lina Tang,[a] Puiki Leung, *[a] Akeel A. Shah,[a] Cristina Flox, [b] Frank C. Walsh[c] and Qiang Liao [a]

A hydroquinone (HQ)/1,2-dihydroxybenzene-3,5-disulfonic acid (Tiron) binary catholyte system is developed for membraneless zinc hybrid flow batteries, leveraging sequential redox reactions with complementary potentials to enhance energy density and electrochemical kinetics. The HQ–Tiron system achieves an energy density of 21.4 W h L^{-1} and a peak power density of 102.3 mW cm^{-2}.

Redox flow batteries (RFBs) offer a promising alternative by decoupling energy and power capacities, enabling long cycle lives and offering improved safety during operation.[1] However, widespread implementation remains hindered by the high capital cost of conventional systems, particularly all-vanadium RFBs.[2] These rely on expensive vanadium salts and perfluorinated ion-exchange membranes, such as Nafion®, which together account for over 30 percent of the system cost and contribute to overall costs of USD 350 to 600 per kW h, significantly above the U.S. Department of Energy's target of less than USD 100 per kW h.[3] Membraneless RFB designs have emerged as a cost-reduction strategy that avoids ion-exchange membranes altogether, using kinetic barriers or spatial redox separation to suppress species crossover.[4] While approaches based on laminar flow or biphasic liquid interfaces have demonstrated feasibility, their small-scale architecture, low throughput and instability under practical conditions have limited progress toward industrial deployment.[5] In contrast, hybrid flow batteries combining soluble redox couples with solid-phase reactions or electrodeposition show greater promise for achieving membrane-free operation at scale.[6] Among these, zinc organic hybrid flow batteries have emerged as a promising candidate due to their low cost and reduced environmental impact. Moreover, designed additives and interface engineering effectively address Zn anode challenges.[7]

These systems typically couple zinc electrodeposition and stripping at the anode with organic redox reactions at the cathode, providing moderate cell voltages (*e.g.* >1.0 V) and simplified architecture without requiring membrane separation.[8] Despite the structural advantages, performance remains constrained by limited solubility of organic active materials, sluggish kinetics and parasitic reactions between the zinc electrodeposits and oxidized catholyte species, which contribute to capacity fade and self-discharge.[9] Improving electrolyte design through molecular-level tuning has therefore become a key strategy for advancing system performance. Recent efforts have shifted toward binary catholyte systems, which combine two redox-active organic molecules to exploit synergistic effects.[10] Strategic molecular pairing enables complementary functions, such as improved solubility, faster charge transfer, broader voltage windows and increased redox reversibility, without requiring complex synthetic modification of the molecules.[11] The synergistic behavior of such redox-active pairings has been shown to enhance both energy and power performance, although binary electrolyte systems remain rare and largely unexplored in practical flow battery designs. This work introduces a novel binary catholyte composed of HQ and Tiron, specifically tailored for membraneless zinc-organic hybrid flow batteries. The HQ–Tiron combination establishes a sequential two-step redox mechanism with complementary redox potentials, effectively broadening the electrochemical operating window and facilitating efficient electron transfer.

The electrochemical and battery performance of metal ion/organics-Tiron binary cathodes were systematically evaluated (Fig. S1–S4, SI), enabling preliminary screening of suitable binary cathode systems. Based on this analysis, the high-performance HQ–Tiron binary cathode was selected for subsequent investigation. As shown in Fig. 1a, the individual solubilities of HQ and Tiron in aqueous media are 0.23 M and 1.57 M, respectively. Notably, the combined HQ–Tiron mixture exhibits an enhanced solubility of up to 1.8 M, which corresponds to a theoretical redox capacity of *ca.*70 A h L^{-1}. This improvement indicates favorable intermolecular interactions that increase the effective concentration of active species in solution. The redox reactions and

[a] *Key Laboratory of Low-Grade Energy Utilization Technologies and Systems, MOE, Chongqing University, Chongqing 400030, China. E-mail: P.leung@cqu.edu.cn*
[b] *Department of Electrical Energy Storage, Iberian Centre for Research in Energy Storage, Campus University of Extremadura, Avda. de las Letras, s/n, 10004 Cáceres, Spain*
[c] *Electrochemical Engineering Laboratory, Department of Mechanical Engineering, Faculty of Engineering and Physical Sciences, University of Southampton, Southampton SO17 1BJ, UK*

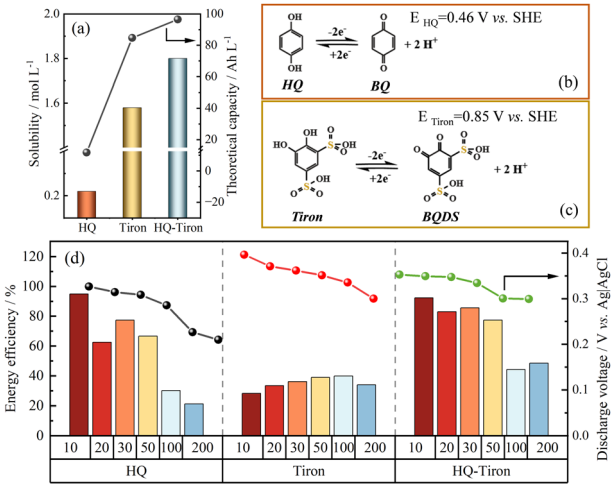

Fig. 1 (a) Solubility and theoretical capacity of HQ, Tiron and the HQ–Tiron binary catholyte; (b) redox reaction of the HQ/BQ couple; (c) redox reaction of the Tiron/BQDS couple; (d) half-cell charge–discharge profiles of HQ, Tiron and HQ–Tiron catholytes at various current densities (10–200 mA cm^{-2}).

associated potentials of the HQ/1,4-benzoquinone (BQ) and Tiron/1,2-benzoquinone-3,5-disulfonic acid (BQDS) couples are illustrated in Fig. 1b and c, respectively. HQ undergoes a reversible two-electron redox reaction with a standard potential of *ca.* 0.46 V *vs.* SHE, while Tiron is oxidized to BQDS at a higher potential of *ca.* 0.85 V *vs.* SHE.[12] These well-separated redox processes enable the sequential electron transfer mechanism that underpins the synergistic behavior of the binary system. Molecular interactions, such as π–π stacking and hydrogen bonding, further enhance redox kinetics and reversibility while mitigating parasitic side reactions.[13] Electrochemical performance, reaction mechanisms and stability characteristics are investigated through a combination of experimental techniques and theoretical analysis. The HQ–Tiron binary catholyte represents a novel electrolyte formulation that delivers enhanced energy and power densities, high coulombic efficiency and stable cycling performance under membraneless conditions. These features indicate its strong potential for practical and scalable deployment in cost-effective stationary energy storage systems.

The practical applicability of the HQ–Tiron binary catholyte in membraneless RFB systems was investigated through a series of galvanostatic charge–discharge tests conducted under various current densities using a cathode half flow-cell. As the current density increased, the voltage profiles (Fig. S5, SI) became broader with slightly increased overpotentials but overall efficiency remained competitive. Even at 50 mA cm^{-2}, the binary system maintained an energy efficiency of approaching 80%, which compares favorably with both HQ- and Tiron-only systems tested under identical conditions, as shown in Fig. 1d. The HQ–Tiron binary system outperformed both single-component systems at nearly all current densities, confirming that the combination of HQ's fast kinetics with Tiron's extended voltage range creates a beneficial tradeoff between energy and power performance. These results demonstrated that the HQ–Tiron binary catholyte system exhibits a synergistic "1 + 1 > 2" performance enhancement compared to individual HQ and Tiron cathodes, primarily attributed to the molecular synergy between HQ and Tiron components.

The enhanced electrochemical performance of the HQ–Tiron binary catholyte was further investigated using a combination of materials characterization, kinetic analysis and theoretical modeling, aimed at elucidating the underlying charge transfer and mass transport mechanisms. Nuclear magnetic resonance (NMR), Fourier transform infrared (FTIR) spectroscopy and scanning electron Microscopy (SEM) analyses reveal the strong intermolecular interactions between HQ and Tiron (Fig. S6–S8, SI). Cyclic voltammetry (CV) across different scan rates revealed that both HQ and Tiron alone followed diffusion-controlled quasi-reversible redox processes (Fig. S9, SI), with linear peak current–scan rate relationships. However, when combined, the HQ–Tiron system exhibited significantly improved reversibility, as evidenced by increased peak currents and reduced peak-to-peak separation. The HQ component retained its original anodic slope (0.084) while exhibiting a more negative cathodic slope (−0.110), indicative of enhanced reduction kinetics. Simultaneously, the Tiron component demonstrated increased anodic current response with little change in cathodic behavior, implying more efficient oxidation but the reduction process likely involved the surface adsorption[14] (Fig. 2a and b). These changes support the hypothesis of a synergistic redox interaction, where HQ and Tiron engage in complementary reactions that accelerate charge transfer dynamics across a broader voltage window.

Supporting evidence from RDE studies confirmed this synergy. All three catholytes (HQ, Tiron and HQ–Tiron) exhibited linear increases in limiting current with the square root of rotation speed, consistent with classical Levich behavior[15] (Fig. 2c, d and Fig. S10–S12, SI). The HQ–Tiron system, however, showed enhanced apparent diffusion coefficients for Tiron (6.97×10^{-6} cm^2 s^{-1} compared to 2.79×10^{-6} cm^2 s^{-1} in isolation), suggesting that molecular interactions between HQ and Tiron promote more efficient mass transport. Additionally, kinetic analysis based on Koutecký–Levich and Tafel models revealed an increased rate constant for Tiron oxidation in the binary system (3.78×10^{-3} cm s^{-1} *vs.* 2.81×10^{-3} cm s^{-1} alone),

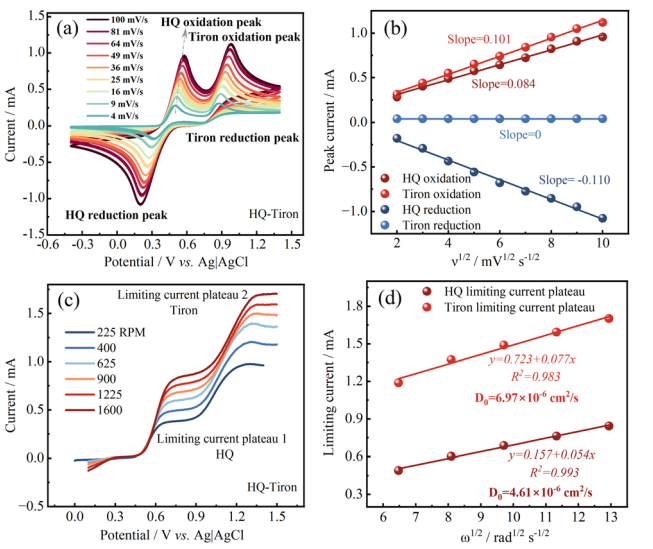

Fig. 2 Electrochemical kinetics of the HQ–Tiron binary catholyte. (a) CV curves at various scan rates; (b) the relationships between peak current and scan rates; (c) linear sweep voltammograms from rotating disk electrode (RDE) measurements; (d) the relationships between the limiting current and rotation speeds.

reflecting the collaborative nature of redox activation in the mixed electrolyte. All data of diffusion coefficients and reaction rate constants are summarized in Table S1, SI.

At the molecular level, density functional theory calculations provided additional insight into the electronic structure of redox-active species. As shown in Fig. 3a, the HQ–Tiron complex displayed a more positive Highest Occupied Molecular Orbital (HOMO) and a nearly Lowest Unoccupied Molecular Orbital (LUMO) compared to Tiron, suggesting enhanced electron-donating ability without compromising electron acceptance. The HOMO–LUMO energy gap narrowed upon oxidation, particularly in HQ–Tiron and HQ–BQDS configurations, indicating facilitated electron transfer during the redox process. Electrostatic potential maps (ESP) revealed electrostatic potential concentrated around hydroxyl and sulfonate groups, forming favorable sites for intermolecular interactions (Fig. 3b). These observations support a mechanism where non-covalent interactions stabilize transition states and reduce energetic barriers to charge transfer. Additionally, the CV curves of the HQ–Tiron binary catholyte at a low scan rate (1.21 mV s^{-1}) revealed two well-resolved successive coupled redox peaks. This is because at lower scan rates, the charge transfer processes at the electrode have sufficient time to proceed, allowing the reaction to approach a state closer to equilibrium. Accordingly, electrochemical impedance spectroscopy in the potential range (0.48–0.52 V *vs.* Ag|AgCl) bridging shoulder peaks exhibited two consecutive charge-transfer semicircles, further confirming the multi-electron transfer characteristics of the HQ–Tiron binary cathode[16] (Fig. S13, SI).

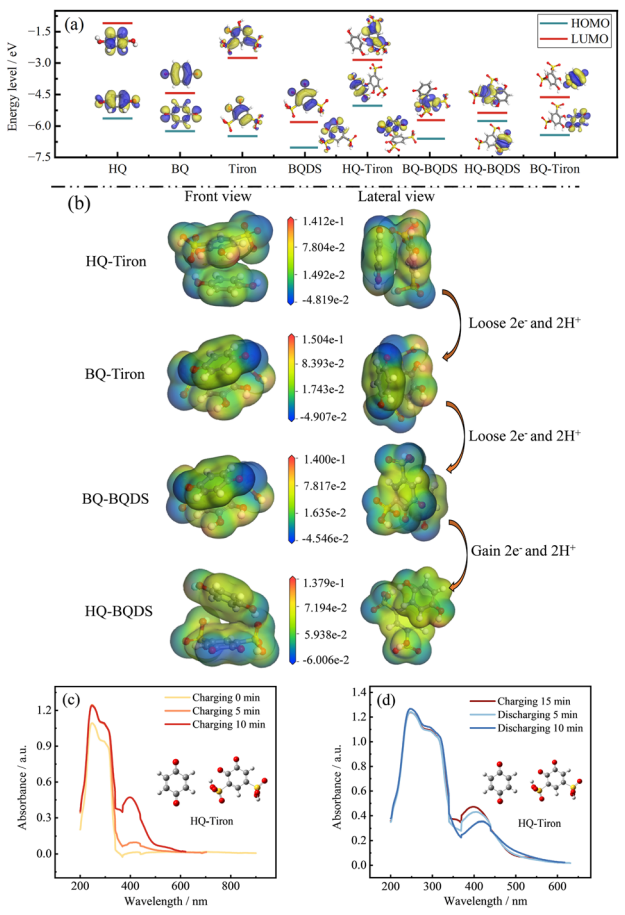

Fig. 3 Electronic structure and spectral analysis of the HQ–Tiron binary catholyte. (a) HOMO–LUMO energy levels of various oxidation states of HQ, Tiron and HQ–Tiron; (b) ESP maps of HQ–Tiron in different oxidation states; (c) UV-vis spectra during charging; (d) UV-vis spectra during discharging.

The proposed interactions were further validated by *in situ* ultraviolet-visible (UV-vis) spectroscopy. During charging, growing absorbance at 400 nm corresponds to the formation of the oxidized Tiron derivative BQDS, while a reversible decrease at 245 nm corresponds to HQ oxidation.[17] Notably, during discharge, the 400 nm absorbance peak exhibited a gradual red shift, indicating a change in the electronic environment and suggesting enhanced π–π interactions between HQ and Tiron (Fig. 3c, d and Fig. S14, SI). These spectral changes align with a reversible ESP structural rearrangement governed by hydrogen bonding and aromatic stacking interactions between HQ and Tiron, as well as can be further confirmed by NMR and FTIR data (Fig. S6 and S7, SI). Meanwhile, molecular dynamics simulations (Fig. S15, SI) revealed that in the HQ–Tiron binary catholyte system, HQ exhibits a lower water coordination number than Tiron, consistent with their respective solubility behaviors in aqueous solution, where Tiron demonstrates higher solubility. Furthermore, fitting the mean square displacement data showed that HQ has a higher diffusion coefficient than Tiron, in agreement with RDE measurements.

As illustrated in Fig. S16 and Table S2, SI, the HQ–Tiron of 1 : 1 composition offered the most favorable tradeoff between capacity retention and energy efficiency, maintaining over 85% of its initial capacity and an energy efficiency exceeding 75%. Under optimal HQ/Tiron molar ratio, extended cycling at 10 mA cm^{-2} over 100 cycles further confirmed the stability of this formulation, achieving a stable coulombic efficiency (CE) above 90% and an average energy efficiency (EE) of *ca.* 81.4% throughout the 100-hour test. The retained discharge capacity exceeded 99.8%, and voltage profiles showed no significant signs of polarization or degradation (Fig. 4a), which is clearly superior to the single HQ or Tiron system (Fig. S17 and S18, SI). The rate capability analysis results (Fig. S19, SI) of the full-cell highlight the high-rate capability of HQ–Tiron, especially given the absence of a membrane, which typically leads to redox mixing and crossover. NMR, FTIR and CV data of the electrolyte after long-cycling test reveal the stability of the HQ–Tiron binary system (Fig. S20–S22, SI). Moreover, SEM images of the electrode surfaces before and after long-cycling tests are shown in Fig. S23, SI, revealing that the surfaces of the Zn anode and carbon felt cathode are uniform and clear, without dendrites or silts. This robust performance is attributed to favorable molecular interactions, such as π–π stacking and hydrogen bonding, which enhance redox reversibility and suppress solute aggregation, while the equimolar ratio limits the accumulation of any single oxidized product, thereby mitigating zinc corrosion and self-discharge.

The binary catholyte also demonstrated a narrow charge–discharge voltage gap and negligible capacity fade at moderate current densities. These characteristics indicate excellent redox reversibility and low resistive losses. Furthermore, polarization and power density curves confirmed that HQ–Tiron supports high current operation with an output power density peaking at 103 mW cm^{-2} at 150 mA cm^{-2} (Fig. 4b), surpassing both HQ and Tiron single-catholyte benchmarks.

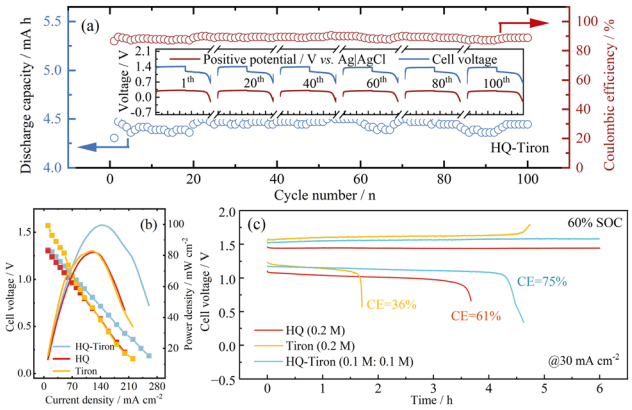

Fig. 4 Full-cell performance of the membraneless Zn-quinones hybrid flow battery. (a) Long-term cycling performance of the HQ–Tiron binary catholyte at 10 mA cm^{-2}; (b) power density curves of HQ, Tiron and HQ–Tiron catholytes; (c) charge–discharge voltage profiles of HQ, Tiron and HQ–Tiron catholytes at 60% SOC.

These trends highlight the advantage of leveraging binary systems to balance and enhance redox dynamics. Overall, the HQ–Tiron binary catholyte achieves efficient and stable operation over a broad current range in membraneless flow batteries. The synergy between HQ's low-potential fast redox and Tiron's high-potential stable oxidation not only broadens the voltage window but also mitigates the limitations of each molecule when used alone. In addition to power performance, the HQ–Tiron system achieves a high energy density of 21.4 W h L^{-1} at a total active species concentration of 1.8 mol L^{-1}, significantly higher than HQ or Tiron alone. This enhancement arises from the broadened voltage window and dual-molecule contribution to redox capacity. As shown in Fig. 4c, the charge–discharge voltage profiles of the HQ–Tiron binary system, HQ- and Tiron single-component system at a high state-of-charge (SOC) demonstrate that the HQ–Tiron binary system achieves a superior CE of 75%, compared to the HQ- or Tiron-only system.

This study presents a membraneless zinc-organic hybrid flow battery utilizing a binary catholyte of HQ and Tiron, which enables stable, efficient and competitive energy storage through sequential liquid-phase redox reactions (Table S3, SI). By coupling zinc electrodeposition at the anode with complementary redox activity at the cathode, the system eliminates the need for ion-selective membranes while maintaining high electrochemical performance. At a 1 : 1 molar ratio, the HQ–Tiron system delivers a peak power density of 103 mW cm^{-2}, an energy efficiency of *ca.* 81.4% over 100 cycles at 10 mA cm^{-2} and capacity retention exceeding 99.8%. These performance gains arise from favorable molecular interactions, including hydrogen bonding and π–π stacking, which enhance redox reversibility, facilitate mass transport and broaden the electrochemical operating window (Fig. S24, SI). Compared to single-component systems, the binary formulation exhibits faster charge transfer, higher diffusion coefficients and more reversible redox behaviors, as confirmed by *in situ* UV-vis spectroscopy and theoretical calculations. This approach demonstrates the potential of molecularly paired organic electrolytes to expand the voltage window, suppress side reactions and improve long-term cycling without requiring complex synthesis or membrane integration. Future work may extend this binary catholyte design to other classes of organic redox-active species to unlock broader voltage tunability, solubility enhancement and molecular-level control across next-generation flow battery chemistries.

Conflicts of interest

There are no conflicts to declare.

Data availability

All data are provided in the SI.

Experimental methods, theoretical/computational details, data tables/figures and additional analyses are available. See DOI: https://doi.org/10.1039/d5cc03528g.

Notes and references

1 (*a*) P. Arévalo-Cid, P. Dias, A. Mendes and J. Azevedo, *Sustainable Energy Fuels*, 2021, **5**, 5366–5419; (*b*) C. Zhang, L. Zhang, Y. Ding, S. Peng, X. Guo, Y. Zhao, G. He and G. Yu, *Energy Storage Mater.*, 2018, **15**, 324–350; (*c*) F. Zhu, W. Guo and Y. Fu, *Chem. Soc. Rev.*, 2023, **52**, 8410–8446.
2 (*a*) R. M. Darling, *Curr. Opin. Chem. Eng.*, 2022, **37**, 100855; (*b*) M. Zhang, M. Moore, J. S. Watson, T. A. Zawodzinski and R. M. Counce, *J. Electrochem. Soc.*, 2012, **159**, A1183.
3 (*a*) L. Tang, P. Leung, M. R. Mohamed, Q. Xu, S. Dai, X. Zhu, C. Flox, A. A. Shah and Q. Liao, *Electrochim. Acta*, 2023, **437**, 141460; (*b*) Z. Huang, A. Mu, L. Wu, B. Yang, Y. Qian and J. Wang, *ACS Sustainable Chem. Eng.*, 2022, **10**, 7786–7810; (*c*) C. Minke and T. Turek, *J. Power Sources*, 2015, **286**, 247–257; (*d*) P. Lv, Z. Cai, B. Zhao, R. Lv, L. Li, H. Chen, P. Jannasch and J. Yang, *Chem. Commun.*, 2025, **61**, 7640–7643.
4 P. Navalpotro, J. Palma, V. Muñoz-Perales, A. Martínez-Bejarano, M. V. Martín-Arroyo, D. P. Taylor, A. Platek-Mielczarek, P. G. Rivano, F. Paratore, E. D. Re and R. Marcilla, *APL Energy*, 2025, **3**, 012001.
5 (*a*) M. O. Bamgbopa, S. Almheiri and H. Sun, *Renewable Sustainable Energy Rev.*, 2017, **70**, 506–518; (*b*) X. Wang, R. K. Gautam and J. Jiang, *Chem. Soc. Rev.*, 2025, **54**, 5895–5911.
6 (*a*) X. Wang, J. Chai and J. J. Jiang, *Nano Mater. Sci.*, 2021, **3**, 17–24; (*b*) A. Khor, P. Leung, M. R. Mohamed, C. Flox, Q. Xu, L. An, R. G. A. Wills, J. R. Morante and A. A. Shah, *Mater. Today Energy*, 2018, **8**, 80–108.
7 (*a*) H. Fan, B. Hu, H. Li, M. Ravivarma, Y. Feng and J. Song, *Angew. Chem., Int. Ed.*, 2022, **61**, e202115908; (*b*) M. Park, E. S. Beh, E. M. Fell, Y. Jing, E. F. Kerr, D. De Porcellinis, M. A. Goulet, J. Ryu, A. A. Wong, R. G. Gordon, J. Cho and M. J. Aziz, *Adv. Energy Mater.*, 2019, **9**, 1900694; (*c*) Y. Tian, Y. An, Y. Yang and B. Xu, *Energy Storage Mater.*, 2022, **49**, 122–134.
8 P. K. Leung, T. Martin, A. A. Shah, M. R. Mohamed, M. A. Anderson and J. Palma, *J. Power Sources*, 2017, **341**, 36–45.
9 (*a*) J. Yin, Y. Tan and J. Pu, *Chem. Commun.*, 2025, **61**, 5857–5870; (*b*) J. Cui, Z. Guo, J. Yi, X. Liu, K. Wu, P. Liang, Q. Li, Y. Liu, Y. Wang, Y. Xia and J. Zhang, *ChemSusChem*, 2020, **13**, 2160–2185.
10 M. Maleki and M.-A. Goulet, *ChemRxiv*, 2025, preprint, DOI: 10.26434/chemrxiv-2025-k697f.
11 K. Lee, K. Amini and M. Aziz, *ACS Energy Lett.*, 2025, **10**, 4067–4073.
12 (*a*) A. Permatasari, W. Lee and Y. Kwon, *Chem. Eng. J.*, 2020, **383**, 123085; (*b*) F. Hasan, V. Mahanta and A. A. A. Abdelazeez, *Adv. Mater. Interfaces*, 2023, **10**, 2300268.
13 (*a*) L. Zhang, Q.-H. Zhu, Y.-R. Zhou, S.-L. Wang, J. Fu, J.-Y. Liu, G.-H. Zhang, L. Ma, G. Tao, G.-H. Tao and L. He, *Nat. Commun.*, 2023, **14**, 8181; (*b*) J.-H. Deng, J. Luo, Y.-L. Mao, S. Lai, Y.-N. Gong, D.-C. Zhong and T.-B. Lu, *Sci. Adv.*, 2020, **6**, eaax9976.
14 G. Yang, Y. Zhu, Z. Hao, Y. Lu, Q. Zhao, K. Zhang and J. Chen, *Adv. Mater.*, 2023, **35**, 2301898.
15 (*a*) J. Park, Y. Lee, D. Yun, D. Kim, G. Hwang, B. Han, Y. Kim, J. Jung and J. Jeon, *Electrochim. Acta*, 2023, 439; (*b*) S. Pang, X. Wang, P. Wang and Y. Ji, *Angew. Chem., Int. Ed.*, 2021, **60**, 5289–5298.
16 A. C. Lazanas and M. I. Prodromidis, *ACS Meas. Sci. Au*, 2023, **3**, 162–193.
17 L. Tong, Q. Chen, A. A. Wong, R. Gómez-Bombarelli, A. Aspuru-Guzik, R. G. Gordon and M. J. Aziz, *Phys. Chem. Chem. Phys.*, 2017, **19**, 31684–31691.